Atmos. Chem. Phys. Discuss., https://doi.org/10.5194/acp-2018-757
Manuscript under review for journal Atmos. Chem. Phys.
Discussion started: 22 August 2018

Atmospheric Chemistry and Physics Discussions

pH-Dependent production of molecular chlorine, bromine, and iodine from frozen saline surfaces

John W. Halfacre[1], Paul B. Shepson[2,3], Kerri A. Pratt[4]

[1]Department of Chemistry, Indiana University Southeast, New Albany, IN USA
[2]Department of Chemistry, Purdue University, West Lafayette, IN USA
[3]Department of Earth, Atmospheric, and Planetary Sciences, Purdue University, West Lafayette, IN USA
[4]Department of Chemistry and Earth & Environmental Sciences, University of Michigan, Ann Arbor, MI USA

Correspondence to: J. W. Halfacre (halfacre@ius.edu)

Atmos. Chem. Phys. Discuss., https://doi.org/10.5194/acp-2018-757
Manuscript under review for journal Atmos. Chem. Phys.
Discussion started: 22 August 2018

Atmospheric Chemistry and Physics Discussions

Abstract

The mechanisms of molecular halogen productions from frozen saline surfaces remain incompletely understood, limiting our ability to predict atmospheric oxidation and composition in the polar regions. In this laboratory study, condensed-phase hydroxyl radicals (OH) were photochemically generated in frozen saltwater solutions that mimicked the ionic composition of ocean water. These hydroxyl radicals were found to oxidize Cl^-, Br^-, and I^-, leading to the release of Cl_2, Br_2, and I_2. This finding is consistent with mechanisms proposed from recent Arctic field studies for observed snowpack molecular halogen production. At moderately acidic pre-freezing pH (buffered between 4.5-4.8), irradiation of ice surfaces containing OH-precursors produced elevated amounts of I_2. Subsequent addition of O_3 produced additional I_2, as well as low amounts of Br_2. At lower pH (1.7-2.2), substantial photochemical production of Br_2 was observed, following rapid dark conversion of I^- to I_2 via reactions with hydrogen peroxide or nitrite. Exposure to O_3 under these low pH conditions also increased production of Br_2 and I_2, possibly through surfaced-based reactions with O_3, or the production and heterogeneous recycling of gas-phase HOBr and HOI. Our results suggest the observed products are dependent on the relative concentrations of halides at the ice surface. Finally, photochemical production of Cl_2 was only observed when the irradiated sample was composed of high-purity NaCl and hydrogen peroxide (acting as the OH precursor) at low pH (~1.8). While OH was shown to produce Cl_2 in this study, kinetics calculations suggest that heterogeneous recycling chemistry may be equally or more important for Cl_2 production in the Arctic atmosphere.

Atmos. Chem. Phys. Discuss., https://doi.org/10.5194/acp-2018-757
Manuscript under review for journal Atmos. Chem. Phys.
Discussion started: 22 August 2018

Atmospheric Chemistry and Physics Discussions

1 Introduction

It is now well-established that gas-phase halogen species influence atmospheric composition through reactions with ozone (O_3), volatile organic compounds (VOCs), and gaseous elemental mercury (Hg^0) (Barrie and Platt, 1997; Carpenter et al., 2013; Platt and Hönninger, 2003; Saiz-Lopez and von Glasow, 2012; Simpson et al., 2007, 2015; Steffen et al., 2008, 2014, and references therein). In polar regions, it is believed that halogens build up to effective concentrations through a heterogeneous reaction sequence known as the "halogen explosion" (Reactions R1-4, where X represents Cl, Br, or I) (Garland and Curtis, 1981; Tang and McConnell, 1996; Vogt et al., 1996; Wennberg, 1999).

$$X_2 + h\nu \rightarrow 2X \quad \text{(R1)}$$

$$X + O_3 \rightarrow XO + O_2 \quad \text{(R2)}$$

$$XO + HO_2 \rightarrow HOX + O_2 \quad \text{(R3)}$$

$$HOX + X^- + H^+ \rightarrow X_2 + H_2O \quad \text{(R4)}$$

In this sequence, a molecular halogen (X_2) is photolyzed to produce two reactive halogen radicals. These radicals can react with O_3 to produce halogen oxides. XO produced in Reaction R2 rapidly photolyzes (or reacts with NO) to regenerate O_3 and X_2 in a null cycle. To irreversibly remove ambient O_3, XO must react with another halogen oxide or Hg^o. Alternatively, XO can react with HO_2 to form HOX (Reaction R3) or NO_2 to form $XONO_2$. Gas-phase HOX can heterogeneously react with salt-laden surfaces, including sea-salt aerosol particles (McConnell et al., 1992) and the "disordered interface" (often referred to as a quasi-liquid or quasi-brine layer) that exists on frozen saline surfaces (Bartels-Rausch et al., 2014; Cho et al., 2002) to produce X_2, effectively returning two halogen radicals to the gas phase. Additionally, this mechanism is enhanced under acidic conditions, confirmed by laboratory studies of aqueous (Fickert et al., 1999) and frozen solutions (e.g., Abbatt et al., 2010; Sjostedt and Abbatt, 2008; Wren et al., 2013), and from field observations (Pratt et al., 2013).

While much has been learned about the atmospheric chemistry of reactive halogen species in the Arctic, knowledge gaps remain in the chemical mechanisms by which molecular halogens are produced on frozen surfaces (Liao et al., 2014; Pratt et al., 2013). However, there have been recent reports of in situ, light-induced production of Cl_2 (Custard et al., 2016), Br_2 (Pratt et al., 2013; Raso et al., 2017), and I_2 (Raso et al., 2017) within snowpack interstitial air, and further suggest that this production is enhanced following the addition of O_3. The Br_2-producing snowpacks studied by Pratt et al. (2013) were characterized as having larger surface area, lower pH ($\leq$ 6.3), greater

71 [Br^-]/[Cl^-] molar ratios (≥ 1/148), and lower salinity relative to other frozen samples collected near Utqiaġvik, Alaska.
72 The proposed mechanism for this chemistry is based on laboratory studies of condensed-phase, hydroxyl radical (OH)-
73 mediated halogen oxidation (Reactions R5-R12), followed by partitioning of the molecular halogen to the gas phase
74 (Abbatt et al., 2010; Knipping et al., 2000; Oum et al., 1998b).

75 $H_2O_2 + h\nu \rightarrow 2\,OH$ (R5)

76 $NO_2^- + h\nu \rightarrow NO + O^-$ (R6)

77 $O^- + H^+ \rightarrow OH$ (R7)

78 $OH + X^- \leftrightarrow HOX^-$ (R8)

79 $HOX^- + H^+ \rightarrow X + H_2O$ (R9)

80 $X + X^- \leftrightarrow X_2^-$ (R10)

81 $2X_2^- \rightarrow X_3^- + X^-$ (R11)

82 $X_3^- \leftrightarrow X^- + X_2$ (R12)

83 Direct, light-induced halogen production from frozen surfaces in the presence of OH has been previously demonstrated
84 in the laboratory for Br_2 and possibly for I_2 (Abbatt et al., 2010), but analogous chemistry for Cl_2 has yet to be observed.
85 Additionally, photochemical production of I_2 has been directly observed in the absence of OH (Kim et al., 2016).
86 Employing cavity ring-down spectroscopy, Kim et al. (2016) reported photochemical production of I_2 from a frozen
87 solution by known aqueous-phase chemistry (R13-17). This proposed photochemical mechanism involves an (I^--O_2)
88 charge-transfer complex (Levanon and Navon, 1969).

89 $O_2(aq) + 4H^+ + 6I^- \rightarrow 2I_3^- + 2H_2O$ (R13)

90 $I^- + O_2 \rightarrow (I^-O_2) \xrightarrow{h\nu} I + O_2^-$ (R14)

91 $I + I^- \leftrightarrow I_2^-$ (R15)

92 $2I_2^- \rightarrow I_3^- + I^-$ (R16)

93 $I_3^- \leftrightarrow I^- + I_2$ (R17)

94 Kim et al. (2016) also report enhanced photochemical I_3^- production (determined spectrophotometrically) from sunlit
95 frozen iodide solutions placed on Antarctic snowpack, as well as from refrozen field snow and glacier samples doped

Atmos. Chem. Phys. Discuss., https://doi.org/10.5194/acp-2018-757
Manuscript under review for journal Atmos. Chem. Phys.
Discussion started: 22 August 2018

Atmospheric Chemistry and Physics Discussions

with iodide. A question is thus raised regarding the necessity of OH for I_2 production under environmentally-relevant conditions.

The role of O_3 in halogen production on frozen surfaces is also unclear. Previous laboratory studies have demonstrated that halide-doped frozen surfaces exposed to O_3 can lead to Br_2 production (independent of radiation, R18-R19, and R4) (Oldridge and Abbatt, 2011; Oum et al., 1998a; Wren et al., 2013).

$$O_3 + Br^- \leftrightarrow BrO^- + O_2 \quad \text{(R18)}$$

$$BrO^- + H^+ \leftrightarrow HOBr \quad \text{(R19)}$$

It has recently been shown that this process proceeds at the surface, through a water-stabilized ozonide, $Br{\cdot}OOO^-$, as shown in reactions R20-R22. Artiglia et al. (2017) observed this $Br{\cdot}OOO^-$ intermediate via liquid-injection X-ray photoelectron spectroscopy.

$$Br^- + O_3 \rightarrow Br{\cdot}OOO^- \quad \text{(R20)}$$

$$Br{\cdot}OOO^- + H^+ \rightarrow HOBr + O_2 \quad \text{(R21)}$$

$$Br{\cdot}OOO^- + H_2O \rightarrow HOBr + O_2 + OH^- \quad \text{(R22)}$$

Wren et al. (2013) found that Cl_2 was produced primarily via heterogeneous recycling of HOCl, resulting from BrCl photolysis, on halide-rich artificial snow. However, the observation that O_3 induces halogen production from frozen surfaces has yet to be confirmed by field observations of snowpack chemistry, in which exposure to only O_3 in the absence of light has not been shown to produce molecular halogens. Such in-situ experiments in the presence of O_3 were shown to produce enhanced molecular halogens only in the presence of light (Custard et al., 2017; Pratt et al., 2013; Raso et al., 2017), raising a question of whether O_3 is more important for initial halogen release, or in a gas phase propagation/recycling capacity (i.e., per the halogen explosion).

In this study, we utilized a custom ice-coated-wall flow reactor in tandem with chemical ionization mass spectrometry (CIMS) to study Br_2, Cl_2, and I_2 production from frozen surfaces with compositions mimicking sea ice. The effects of photochemically generated OH radicals, O_3 addition, and pH are tested as they relate to the production of these halogens. Surface pH was controlled through use of buffers.

Atmos. Chem. Phys. Discuss., https://doi.org/10.5194/acp-2018-757
Manuscript under review for journal Atmos. Chem. Phys.
Discussion started: 22 August 2018

2 Methods

2.1 Materials

Sample solutions were composed to mimic the halide composition of seawater. This was achieved using either dissolved Instant Ocean (Spectrum Brands), or commercially available halide salts at a composition that mimics Instant Ocean (for consistency) in solutions referred to hereafter as "saltwater." The halide concentrations in these solutions were made to a final concentration of 0.56M Cl^-, 7.2 x 10^{-4} M Br^-, and 1.9 x 10^{-6} M I^-. Except for Instant Ocean, all chemicals were purchased from Sigma Aldrich. Halide salts include solid NaCl (puriss. p.a. grade, ≥99.5% purity), NaBr (puriss. grade, >99% purity), KI (puriss. p.a. grade, ≥99.5% purity). Sigma Aldrich lists an I^- impurity in the NaCl salt of ≤ 10 mg/kg, but the initial aqueous concentration of I^- in this solution could not be confirmed by ion chromatography. We note that these halide concentrations are comparable to those in actual seawater (Herring and Liss, 1974; Luther et al., 1988; Tsunogai and Sase, 1969), which typically contains Cl^-, Br^-, and I^- at ratios of $1:{}^1/_{660}:{}^1/_{200,000}$. Solutes were dissolved in ultrapure water (Birck Nanotechnology Center). Dissolved organic carbon for Instant Ocean and halide salt solutions were analyzed using a Shimadzu TOC-V_{CSH} Total Organic Carbon Analyzer, and determined at approximately 70 mg/L for Instant Ocean solutions, and less than 5 mg/L for saltwater solutions. No further characterization of carbon-containing compounds was performed.

While previous investigators have adjusted the pre-freezing pH of their samples, it is very difficult to know the pH in the disordered interface of frozen samples (Bartels-Rausch et al., 2014), though there is evidence from laboratory studies suggesting that the pH of salt solutions remains largely unchanged after freezing (Wren and Donaldson, 2012b). To obviate this problem, the aqueous solutions used in this study were buffered so that the same pH will exist in the frozen disordered interface. All solutions were buffered by either 20 mM acetic acid (ACS reagent grade, ≥99.7% purity)/acetate (puriss. p.a. grade) buffer (pH ≈ 4.5-4.7), or 20 mM bisulfate (ReagentPlus grade, 99% purity)/sulfate (ReagentPlus grade, ≥ 99.0% purity) buffer (pH ≈1.7 – 2.0). pH values of sample solutions were determined before and after experiments, with no significant changes observed. 100 μM of either hydrogen peroxide (trace analysis grade, ≥ 30% purity) or sodium nitrite (ReagentPlus grade, ≥ 99.0% purity) were included as photochemical hydroxyl radical precursors, via reactions R5, and R6-7.

2.2 Flow tube

Experiments were carried out in a custom-built 150 cm long, 2.5 cm ID frozen-walled Pyrex flow tube contained within a temperature-controlled cooling jacket. In each experiment, 80.0 mL of sample solution was poured into the tube, which was subsequently sealed with vinyl caps (McMaster-Carr). The flow tube was then rotated on motorized rollers within a 170 cm x 50 cm x 50 cm, insulated wooden cooling chamber. Crushed dry ice was placed along the bottom of the chamber, and fans were used to circulate the air throughout the chamber such that the flow tube was evenly cooled. After ~30 minutes, the sample was evenly frozen (ice thickness of 0.9 mm). The flow tube was subsequently transferred to an enclosed 156 cm x 50 cm x 50 cm wooden, Mylar-lined experiment chamber, and connected to a recycling chiller set to 258 K (i.e., above the $NaCl{\bullet}2H_2O$ eutectic point). The cooling liquid used for the chiller was a mixture of 60% ethylene glycol and 40% distilled water. Six UVA-340 solar simulator lamps (Q-Labs, 295 – 400 nm with maximum wattage at 340 nm) were installed in the experiment box (two on each side except bottom). Each side was lined with reflective Mylar sheets to evenly irradiate the flow tube when the lamps were powered.

A flow schematic representing typical experiments is shown in Fig. 1. The carrier gas (Air, Ultra Zero grade, Praxair) was scrubbed of volatile organic compounds using activated charcoal, and water by travelling through coiled stainless-steel tubing surrounded by crushed dry ice (replaced throughout the course of an experiment). This gas was measured to contain $\leq$ 300 – 400 pmol mol^{-1} NO (experimentally determined limits of detection) using the Total REactive Nitrogen Instrument (TRENI) (Lockwood et al., 2010; Xiong et al., 2015). Though NO_2 was not measured, we believe it would have been removed by the charcoal trap. Before entering the experiment coated-wall flow tube, the carrier gas flowed through a commercial O_3 generator (2B Technologies model 306). Carrier gas air entered the tube near room temperature (20 ^oC). At the start of experiments, the O_3 generator was set to 0 nmol mol^{-1}. Carrier gas then entered the flow tube in the dark experiment chamber. In most experiments, the carrier gas was regulated to a volumetric flow rate of 4.0 L min^{-1}, which yields a residence time in the flowtube of ~12 seconds. On exiting the flow tube, sample air was characterized using a Thermo Environmental 49i O_3 monitor (flow rate of ~1.5 L min^{-1}) and a chemical ionization mass spectrometer (CIMS, sampling flow rate of ~1.7 L min^{-1}, described below in Sect 2.3). Excess flow air was vented away. At set times in an experiment, the solar simulator bulbs were activated, and O_3 was added to the system by powering the O_3 generator.

Atmos. Chem. Phys. Discuss., https://doi.org/10.5194/acp-2018-757
Manuscript under review for journal Atmos. Chem. Phys.
Discussion started: 22 August 2018

172 **2.3 CIMS**

173 Halogen species were detected using a chemical ionization mass spectrometer (CIMS), described previously
174 by Liao et al. (2011) and Pratt et al. (2013). Chemical ionization is achieved by ion-molecule reactions that occur
175 between iodide-water reagent clusters, $I(H_2O)_n^-$ in N_2, and the gas-phase sample in zero air. The iodide-water clusters
176 are formed when gas-phase iodide ions, generated by flowing 5 ppm methyl iodide through a ^{210}Po ionizer (NRD)
177 combines with water in the humidified ion-molecule region of the CIMS. Ion were filtered using a quadrupole mass
178 filter. The ice-coated flowtube was connected to the CIMS via approximately 50 cm of i.d. 1/2″ PFA Teflon tubing.

179 A typical CIMS sampling cycle consisted of an 8.35s duty cycle. Dwell times for all monitored species were
180 250 ms with the exception of the reagent ion (detected as *m/z* 147, $I(H_2{}^{18}O)^-$), which was set to a dwell time of 100
181 ms. The 18 ions analyzed in this study are listed in Table 1, but we focus herein on results concerning masses related
182 to Br_2 (*m/z* 285 and 287: $I^{79}Br^{79}Br^-$ and $I^{81}Br^{79}Br^-$, respectively), Cl_2 (*m/z* 197 and 199: $I^{35}Cl^{35}Cl^-$ and $I^{37}Cl^{35}Cl^-$), and
183 I_2 (*m/z* 381: I_3^-). In addition, IBr (*m/z* 333 and 335: $I^{79}IBr^-$, $I^{81}IBr^-$) was unambiguously detected in some experiments.
184 The presence of Br_2, Cl_2,and IBr was confirmed by measuring the ratios between the two isotope signals for each
185 mass, compared to the natural abundances (i.e., 1.95 for *m/z* 287:285; 1.54 for *m/z* 197:199; and 1.03 for *m/z* 333:335,
186 respectively). Data outside ±25% the appropriate isotope ratio were excluded from analysis. The isotope ratios for
187 BrCl (*m/z* 241 and 243: $I^{79}Br^{35}Cl^-$, $I^{81}Br^{35}Cl^-$, $I^{79}Br^{37}Cl^-$) masses were never observed at the correct values (1.3 for *m/z*
188 243:241), and so those data were not reported here. As the introduction of ~60 nmol mol^{-1} O_3 to the experimental
189 system significantly increases the background signal for the primary Cl_2 isotope (*m/z* 197, $I^{35}Cl^{35}Cl^-$), the study of Cl_2
190 is limited under these conditions, due to lack of isotopic confirmation of its presence. Though *m/z* 201 ($I^{37}Cl^{37}Cl^-$) was
191 additionally monitored, no Cl_2 was measured above the limit of detection of 1.1 ± 0.2 pmol mol^{-1} for *m/z* 199 with the
192 appropriate isotope ratios in experiments with added O_3 (6.2 for *m/z* 199:201).

193 CIMS calibrations were performed using I_2, Br_2, and Cl_2 permeation devices (VICI) at the start and
194 conclusion of each experiment. Br_2 and Cl_2 permeation outputs were quantified using the spectrophotometric method
195 described by Liao et al. (2012). The I_2 permeation output was quantified by flowing the I_2 through an impinger
196 containing a $NaHCO_3$ (30mM)/$NaHSO_3$ (5mM) reducing solution. This solution quantitatively reduces I_2 to I^-, which
197 was then determined using a Dionex DX500 ion chromatography system. Permeation rates were calculated for each
198 experiment and found to average (1.9±0.1) x 10^{-11}, (5.5±0.1) x 10^{-10}, and (8.6±0.1) x 10^{-10} mol min^{-1} of I_2, Br_2, and

Cl_2, respectively (uncertainties representing standard error of the mean). CIMS calibration factors were calculated for individual experiments. These factors are based on the average of the signal sensitivities, determined from the permeation sources, calculated at the start and completion of each experiment. Corresponding uncertainties for these calibration factors thus represent the 1σ standard deviation of the mean sensitivity. In addition, the sensitivity for HOBr (as $IHOBr^-$) species is assumed to be a factor of 0.5 ± 25% the *m/z* 287 Br_2 sensitivity (Liao et al., 2012), though $IHOBr^-$ was not unambiguously observed according to isotope ratios due to an interference at *m/z* 223 ($IHO^{81}Br^-$). An approximate $I^{79}IBr^-$ calibration factor was assumed to be the average of the sensitivities for *m/z* 287 (IBr_2^-) and 381 (I_3^-). Background measurements were performed before and after the experiment (minimum of 5 min) by passing the carrier gas through the experimental flow tube (without O_3, in the dark), and subsequently through a glass wool scrubber, previously shown to remove molecular halogens with greater than 95% efficiency (Liao et al., 2012; Neuman et al., 2010). Temporal variations in bromine-species signals while using the low pH sulfate/bisulfate buffer were observed in some experiments (Fig. S1) and are discussed in the Supplementary Information.

Analysis of experimental data was based on one-minute averages, with uncertainties representing the standard deviation of these averages. Subsequently, signals were converted to concentrations using the sensitivities calculated above, propagating the sensitivity uncertainty into the measurement uncertainty. Average limits of detection (3σ) across all experiments for the molecular halogens during background periods were 1.8 ± 0.4, 1.2 ± 0.3, and 9 ± 2 pmol mol^{-1} for Br_2, Cl_2, and I_2 respectively (uncertainties representing standard error of the mean). Additionally, reported uncertainties for integrated amounts of formed halogens are calculated as integrated halogen concentrations multiplied by the relative uncertainty in the CIMS signal sensitivity.

3 Results

The experiments described here address the extent to which OH radicals in the condensed phase can lead to I_2, Br_2, and Cl_2 production through condensed-phase reactions within frozen saline surfaces, as hypothesized from recent field (Custard et al., 2017; Pratt et al., 2013; Raso et al., 2017) and laboratory experiments (Abbatt et al., 2010). In addition, we test the pH-dependence of this chemistry, and whether O_3 can enhance this production. We find the relative and absolute amounts of I_2, Br_2, and Cl_2 produced from ice are a complex function of the relative concentrations of the precursor halide ions, the pH, presence of oxidants, radiation, and O_3.

The ice-coated flow tube experiments started under dark conditions and without addition of O_3 (Sect. 3.1). Once signals stabilized, lights were activated for 1-2 h (Sect. 3.2, Sect. 3.3), after which the ozone generator lamp was activated to generate ~60 nmol mol^{-1} of O_3 in the carrier gas to test the impacts of both radiation and ozone (Sect. 3.4). Saline surfaces tested include frozen Instant Ocean (IO) solutions, solutions composed of dissolved reagent grade salts mimicking saltwater (SW) composition, and 0.56 M high purity NaCl (CL1). Unless otherwise specified, integrated amounts of produced halogens represent amounts produced over the course of 1 h of exposure to light (Sect. 3.2, Sect. 3.3) and/or ozone (Sect. 3.4). Many of the salient features of our results are demonstrated by example experiments shown in Fig. 2, which shows the impact of irradiation in the presence of ice phase OH radical precursors, varied pH, and the presence of O_3. Below we discuss the details of our experiments, organized by the mechanism of halogen production and halogen products themselves.

3.1 Dark reaction production of I_2

To photochemically create condensed-phase hydroxyl radicals, either hydrogen peroxide (H_2O_2) or nitrite (NO_2^-) were added to salt solution samples, as they have been estimated to account for 96% of snowpack photochemical OH formation at Utqiaġvik, AK (France et al., 2012). However, both H_2O_2 and NO_2^- can directly convert I^- to I_2 under dark acidic conditions. No dark production of Br_2 or Cl_2 was observed in these experiments for any pH, or presence of OH precursor. The oxidation of I^- by H_2O_2 occurs through the condensed phase reactions R23 and R24 (Küpper et al., 1998):

$$I^- + H_2O_2 \leftrightarrow HOI + OH^- \quad \text{(R23)}$$

$$HOI + I^- + H^+ \rightarrow I_2 + H_2O \quad \text{(R24)}$$

Nitrite ions react with hydronium ions to form the nitroacidium ion, H_2ONO^+, which has been previously shown to produce I_2 (R25-R27) (measured spectrophotometrically as trihalide species, which exist in equilibrium with X_2, as in R12, R17) (Hellebust et al., 2007; O'Driscoll et al., 2006, 2008; O'Sullivan and Sodeau, 2010):

$$NO_2^- + H_3O^+ \leftrightarrow HONO + H_2O \quad \text{(R25)}$$

$$HONO + H_3O^+ \leftrightarrow H_2ONO^+ + H_2O \quad \text{(R26)}$$

$$2\,H_2ONO^+ + 2I^- \leftrightarrow 2NO + I_2 + 2H_2O \quad \text{(R27)}$$

The pH ≤ 2 experiments in this work favor the forward reactions that produce I_2 (R23-24, R25-27).

Atmos. Chem. Phys. Discuss., https://doi.org/10.5194/acp-2018-757
Manuscript under review for journal Atmos. Chem. Phys.
Discussion started: 22 August 2018

Atmospheric Chemistry and Physics Discussions

During the initial connection of the flowtube to the CIMS that would initiate the start of an experiment, a large I_2 signal (measured as I_3^-, *m/z* 381) was observed in several cases in which OH-radical precursors were utilized (e.g., Fig. S2, Fig. 2b). This I_2 production likely originated from the above reactions (R23-27). This signal subsequently decayed as I_2 flushed out of the system until reaching a steady state. Integrated sums of dark I_2 production are estimated in Table S1. However, these amounts represent lower limits of the true sums of dark-produced I_2; while the flow tube is sealed during the freezing of the salt solutions, this seal is removed during connection to the experimental flow path (Fig. 1), making it impossible to accurately determine the extent of I_2 production prior to irradiation.

At pH ≈ 4.7, dark I_2 production was modest, only noticeably affecting experiment IO2 (Fig. S2). In that case, the integrated sum of I_2 released on connection of the flow tube to the CIMS until stabilization was 0.8 (± 0.1) nmol, corresponding to approximately 0.5% of the total 152 nmol I^- available for reaction from the Instant Ocean solution (Table S1). At lower pH (<2), larger amounts of I_2 were observed in the dark immediately upon flow tube connection to the CIMS (i.e., before addition of light and O_3; Fig. 2b). Dark production of I_2 could cause significant depletion of I^-, as Experiments IO4 and SW5 (both using H_2O_2) only have, at most, ~46% of the initial 152 nmol of I^- by the time lights are initiated. These values were calculated by subtracting twice the integrated sums of I_2 produced prior to irradiation (Table S1; i.e., two I^- for every I_2) from the total number of I^- moles in the original IO or SW solutions. Considerably less I_2 production occurred in the dark using NO_2^- as an OH precursor (depleting I^- by an average of 4.5%, Table S1). As will be discussed in Sect. 3.3, following depletion of I^- from the salt solutions, Br_2 was the primary halogen produced at low pH.

3.2 Hydroxyl radical-induced halogen production at pH ≈ 4.7

Integrated amounts of photochemically produced molecular halogens are presented in Table 2 for all experiments. Integration times for calculated halogen production span one hour, beginning at the time lights were activated until 60 minutes later, and in the absence of O_3. At pH ≈ 4.7, experiments without hydroxyl radical precursors (IO6-IO7, SW6-SW7; Table 2) produced amounts of molecular halogens below their respective LODs from the saline ice surfaces after activation of lights. Experiment IO7 was an exception, however, producing 0.11 ± 0.06 nmol of I_2.

In the presence of H_2O_2 at pH ≈ 4.7, I_2 mole fractions increased rapidly upon irradiation, as shown in Fig. 2a. Of the four experiments performed in these conditions (IO1, IO2, SW1, SW2), three experiments (IO1, SW1, SW2)

produced statistically similar amounts of I_2 (mean: 8 ± 2 nmol) after one hour of irradiation (Table 2). Experiment IO2 (Fig. S2), while experimentally identical to IO1, appears to have produced ~10 times less I_2 during this hour after the lights were turned on. However, I_2 was already present prior to turning on the lights, suggesting production originating from the direct reaction between I^- and H_2O_2 (Sect. 3.1). Experiment IO2 otherwise eventually qualitatively resembles the other three analogous experiments (IO1, SW1, SW2; e.g. Fig. 2a) with the I_2 concentration eventually increasing after irradiation (Fig. S2).

Regarding other molecular halogens, IBr was observed upon radiation during Experiment SW2 (Fig. 2a) above the estimated limits of detection (3 pmol mol^{-1}) starting approximately 20 minutes before the addition of O_3. No direct (OH-induced) photochemically produced Br_2 was unambiguously observed at this pH. The apparent photochemical integrated Br_2 sum of 0.034 ± 0.003 nmol reported for experiment IO2 (Table 2) stems from a real signal just above the limit of detection (1.8 ± 0.4 pmol mol^{-1}), and this baseline signal does not change on addition of light. This signal, however, remains below limits of quantitation and should not be considered further. Cl_2 mole fractions remained below limits of detection in all cases with OH-precursors at this pH.

3.3 Effects of the hydroxyl radical on halogen production at pH < 2

It is expected that halogen production will be enhanced when pH is decreased based on reactions R4-R22. In cases without OH precursors at pH < 2, photochemical I_2 production was observed (integrated production of 14 ± 10 nmol for IO8, and 6.0 ± 2.0 nmol for SW8) (Table 2), in contrast to experiments performed at pH = 4.7 in which very little was produced. This production likely stems from the mechanisms outlined by Kim et al. (2016) (R13-17), which requires only light and oxygen to form a charge-transfer complex that results in I_2 production (discussed in Sect. 1). Molecular Br_2 and Cl_2 concentrations remain below limits of detection, consistent with Abbatt et al. (2010), in which no Br_2 or Cl_2 was observed without an OH-precursor.

As discussed in Sect. 3.1, inclusion of H_2O_2 or NO_2^- can result in direct oxidation of I^-, thereby reducing the available [I^-] for photochemical OH oxidation when pH < 2. When H_2O_2 was used as an OH precursor, photochemical production of I_2 across experiments yielded ≤ 0.82 nmol (IO4, IO5, and SW5), likely due to the dark I_2 production mechanisms. When instead NO_2^- was used (as in IO3 and SW3, SW4), initial observations of I_2 on flowtube connection to CIMS were as much as 90% less than when H_2O_2 was used (Table S1). For experiment IO3, the reduced pH enhanced I_2 production (39 ± 1 nmol) compared to the high pH cases (Experiments IO1-2, SW1-2, ranging from

0.6 ± 0.4 to 9 ± 3 nmol) (Table 2). The corresponding seawater experiments were not as conclusive; experiment SW3 only yielded 4.0 ± 0.1 nmol of photochemical I_2 (Fig. S4). Experiment SW4 did not produce any photochemical I_2 and qualitatively resembles the low pH H_2O_2 cases. It is possible that for SW3 and SW4 more I_2 was produced by dark reactions and flushed out of the tube during connection with the CIMS and was therefore not measured.

When $[I^-]/[Br^-]$ approximates the initial conditions of Instant Ocean (~2.6 x 10^{-3}; i.e., IO1-IO3, SW1-SW3), OH-mediated I_2 production precedes Br_2 and IBr production. This initial photoproduction of I_2 is observed for IO4, as shown in the inset of Fig. 2b. Figure 2b shows a delay in Br_2 production until I^- was removed as I_2 (and IBr). After $[I^-]/[Br^-]$ has sufficiently decreased, Br_2 eventually becomes the dominant photochemical product, yielding an average of 4.5 ± 0.5 nmol from IO4 and IO5, and 6.0 ± 0.7 nmol from SW5, all of which used H_2O_2 as an OH precursor, and 5.4 ± 0.7 nmol from SW4, which used NO_2^- as an OH precursor. Simultaneous production of IBr was observed as well (Fig. 2b) when $[I^-]/[Br^-]$ had been reduced following I_2 production. Given the initial depletion of I^- from dark I_2 production (Sect. 3.1), we can estimate $[I^-]/[Br^-]$ at pH < 2 in ice with H_2O_2 just before irradiation based on the remaining moles of I^- in solution (Table S1) and the initial moles of Br^- (calculated using the initial experiment solution volume and concentration of Br^- of 7.2 x 10^{-4} M). $[I^-]/[Br^-]$ was calculated as (1.6 ± 0.7) x 10^{-4}, which is an average calculated for experiments IO4-5 and SW5, and was sufficiently low to result in photochemical production of Br_2.

Photochemical Cl_2 production was only observed from a frozen solution of "pure" NaCl and H_2O_2 at pH=1.8 (CL1), as shown in Fig. 2c. When the lights were turned on, a slight increase in I_2 and IBr were observed in concert with a rapid rise in Br_2, likely resulting from an I^- impurity in the NaCl salt. After about one hour of apparent equilibrium, I_2 concentrations begin decreasing, while Br_2, IBr, and Cl_2 continue rising. Over one hour of illumination, 93 ± 3 pmol of Cl_2, 100 ± 10 pmol of Br_2, and 100 ± 10 pmol of I_2 were measured. However, as shown in Fig 2c, the greatest rate of increase in signal did not occur until t = 1 h (after irradiation). Integrating instead from t=0 until t=2 hours, the amount of Cl_2 produced was 190 ± 10 pmol, while the amount of Br_2 increased to 310 ± 20 pmol. The initial $[Br^-]$ of the CL1 solution was determined to be (4.5 ± 0.3) x 10^{-6} M via ion chromatography, meaning Cl_2 production was observed at $[Br^-]/[Cl^-]$ of 8.1 x 10^{-6} ($^1/_{124,000}$), compared to the Instant Ocean $[Br^-]/[Cl^-]$ of ~ $^1/_{800}$. Unfortunately, BrCl could not be observed due to an unknown interference at *m/z* 241 and 243.

Atmos. Chem. Phys. Discuss., https://doi.org/10.5194/acp-2018-757
Manuscript under review for journal Atmos. Chem. Phys.
Discussion started: 22 August 2018

3.4 Effects of O_3 on halogen production

In experiments without an OH source (IO6-IO8, SW6-SW8), I_2 production was greatest when O_3 was introduced to the irradiated tube for both pH regimes (Table 2). The amount of I_2 produced in these experiments was large, ranging from 26 ± 9 nmol to 80 ± 1 nmol at pH = 4.7, and from 2.6 ± 1.7 nmol to 38 ± 12 nmol at pH < 2. While the I_2 produced pH < 2 appears to be lower, I_2 had already been produced prior to addition of O_3 (i.e., with only light as a stimulant, Sect. 3.3), yielding a lower $[I^-]/[Br^-]$ ratio when O_3 was eventually added. Br_2 production amounts ranged from 0.012 ± 0.001 nmol to 0.16 ± 0.01 nmol at pH = 4.7 and taking up to 6 hours to raise above detection limits after O_3 was added. At pH ≤ 2, Br_2 production amounts ranged 0.14 ± 0.02 nmol to 0.93 ± 0.05 nmol, in the absence of an OH source.

When OH-precursors were present, the addition of O_3 to the zero-air flow over the irradiated frozen sample caused additional production of I_2 and Br_2, as shown in Figure 2a and b, under both pH conditions (pH ≤ 2, pH = 4.7) (Table 2). I_2 integration times here represent one hour, beginning at the time when O_3 is introduced until 60 minutes later. In experiments at pH ≈ 4.7 in which $[I^-]/[Br^-]$ remained sufficiently large due to minimal dark production of I_2 (i.e., IO1-2, SW1-2), exposure to O_3 caused a sharp increase in I_2 (as in Fig. 2a). I_2 production amounts for frozen Instant Ocean at pH ≈ 4.7 (IO1, IO2) average 22 ± 10 nmol, about two times less than for frozen saltwater experiments SW1 and SW2 (average production amount of 51 ± 25 nmol). As the I_2 signal decayed, the corresponding Br_2 signals gradually increased above detection limits, approximately 3h after the introduction of O_3 (Fig. 2a). The average integrated amounts of Br_2 produced from these pH ≈ 4.7 experiments were very similar (0.05 ± 0.01 nmol for IO experiments and 0.03 ± 0.01 nmol for SW experiments).

When pH < 2, the effects of O_3 addition varied according to the remaining availability of I^-. When the surface I^- reservoir had been reduced from dark reactions with H_2O_2 or NO_2^- (R17-21; Sect. 3.1), exposure to O_3 did not increase I_2 above the LOD in all experiments except IO5, which exhibited a small spike before decaying below the LOD (0.11 ± 0.06 nmol in IO5). However, O_3 did cause additional Br_2 production after one hour (average of 10 ± 2 nmol for IO4 (Fig. 2b) and IO5, and 14 ± 2 nmol for SW4 and SW5). In contrast, for SW3 (using NO_2^- as an OH source), there was relatively little initial consumption of I^- by dark reaction; therefore, when O_3 was added, an amount of I_2 equal to 1.1 ± 0.1 nmol was observed, comparable to what was observed with the higher pH experiments (Fig. S4). The amount of Br_2 produced (0.46 ± 0.01 nmol) was also significantly less than observed when I^- was initially depleted, demonstrating the importance of the halide ratios (see Section 4.2). Unfortunately, the addition of O_3

introduced a strong interference for the signal observed at *m/z* 197 ($I^{35}Cl^{35}Cl^-$) rendering Cl_2 isotopic ratios invalid, and hence no information regarding the relationship between Cl_2 and O_3 could be ascertained for any experiments involving O_3.

HOX compounds were also observed when O_3 was present, likely formed in the flowtube by O_3 reactions with halides as in R18 and R19 (Fig. 3-4; discussed in more detail in the Supplemental Information). Figure 3 shows this for IO2 (pH=4.7 experiment using Instant Ocean, analogous to SW2 in Fig. 2a, as well as IO1 and SW1). For each experiment in this series (pH=4.7 with OH-precursors), increases in I_2, HOI, and Br_2 were readily observed when the O_3 was introduced at hour 2 (Fig. 3). However, corresponding HOBr production was not observed, perhaps either due to a high LOD, or the relatively low abundance of Br_2 that would limit production of HOBr. Conversely, in pH ≤ 2 cases when substantial portions of I^- had already reacted prior to irradiation (IO4, IO5, SW4, SW5), the addition of O_3 produced negligible amounts of I_2 and HOI (Fig. 4). But, in these cases, following the addition of O_3, HOBr (*m/z* 225 $IHO^{81}Br^-$), was observed together with Br_2 (Fig. 4). We note in this case that *m/z* 223, representative of $IHO^{79}Br^-$, does not appear to show an enhancement when O_3 is added to the system. There was a much higher background signal for *m/z* 223 compared with *m/z* 225 ($IHO^{81}Br^-$) resulting from an unknown interference.

4 Discussion

4.1 Role of OH in halogen production in ice

The observations in this study indicate competition for the OH radical in which the most oxidizable halide is oxidized, and the corresponding molecular halogens are produced until that halide is depleted at the surface. The trends in molecular halogen production show acid-enhanced production mechanisms, in which the dominant products are largely dependent on relative halide ratios. These results are consistent with in situ observations of Br_2, BrCl, and Cl_2 formation (Custard et al., 2017; Pratt et al., 2013). In the case of this work, Br_2 and IBr were not observed until I_2 production sufficiently decreased the $[I^-]/[Br^-]$ ratio, and Cl_2 was not observed unless the $[Br^-]/[Cl^-]$ ratio was sufficiently low ($[Br^-]/[Cl^-] = 8.1 \times 10^{-6}$ in this study). This observation is consistent with other lab studies (Abbatt et al., 2010; Sjostedt and Abbatt, 2008). Sjostedt and Abbatt (2008) exposed frozen salt solutions to gas-phase OH and found peak BrCl production occurred as Br^- decreased from an initial $[Br^-]/[Cl^-]$ of 7.3×10^{-5}. Abbatt et al. (2010) generated condensed phase OH on frozen surfaces from photolysis of nitrate, and similarly found lower Br_2 and IBr

integrated amounts at lower $[Br^-]/[Cl^-]$ when temperatures were warmer than the eutectic point of sodium chloride. However, the I^- in Abbatt et al. (2010) originated from impurities in their sodium chloride and sodium bromide reagents and was not quantified, making the relative ratios regarding I^- not quantifiable.

As a first approximation, we estimate via Eq. (1) effective relative reaction rate constants (k_{X^-}/k_{Y^-}, where X and Y represent Br, Cl, or I) for reaction of a halide with OH radicals, assuming that the observed X_2 flux out of the ice is proportional to the production rate (i.e., X_2 desorbs as it is produced, within the residence time of the flow tube), and that oxidation by OH is the rate limiting step:

$$\frac{\text{Flux}_{X_2}}{\text{Flux}_{Y_2}} = \frac{k_{X^-}[X^-][OH][H^+]}{k_{Y^-}[Y^-][OH][H^+]} \quad (1)$$

The assumption that OH oxidation is rate limiting is based on individual I_2 and Br_2 photochemical production amounts between Instant Ocean and saltwater solutions not being statistically different (i.e., the organic matter in Instant Ocean does not appear to impact halogen production), and its dependence on radiation and presence of an OH precursor. The initial molecular halogen flux is calculated as the integrated sum of X_2 (in moles) divided by both integration time (t = 0-3 minutes, starting from the beginning of irradiation to capture the initial flux) and the surface area of ice coverage in the flow tube. The surface area, as well as the [OH] and $[H^+]$ in the "disordered interface" would be identical within individual experiments and cancel in these calculations. The halide ion concentrations (defined in Sect. 2) allow us to solve for the effective relative rate constant, k_{X^-}/k_{Y^-} by assuming the ratios of the halide concentrations are the same as in the pre-freezing solution. At pH = 1.8, we estimate $k_{Br^-}/k_{Cl^-} = (2.4 \pm 0.2) \times 10^5$ from experiment CL1, or, in other words, production of Br_2 is 240,000 times more efficient than production of Cl_2 via (OH + halide) in the surface layer. Across the six experiments performed at pH < 2 (average of 1.85) using Instant Ocean (IO3, IO4, IO5) and saltwater (SW3, SW4, SW5), we calculate an average k_{I^-}/k_{Br^-} of $(9 \pm 4) \times 10^3$ (reported uncertainty is the standard error of the mean, and thus only represents the experiment repeatability).

The above relative rate constant calculations are considered upper limits since the halide ratios used represent those in the pre-freezing solution. In other words, it is assumed that the ions are excluded to the disordered interface in amounts proportional to their pre-freezing concentration. Malley et al. (2018) recently demonstrated that brine can be distributed throughout ice in channels, suggesting that only the solutes at the liquid-air interface (a fraction of the total pre-freezing solution) participate in heterogeneous chemistry. Indeed, we find evidence here suggesting not all ions are available for reaction at the disordered interface surface, particularly experiments for which we lost little I^-

411 from dark I_2 production mechanisms (i.e., pH = 4.7 with OH precursors: IO1, IO2, SW1, SW2). Considering
412 experiment IO2 as an example (Fig. S5), integration of the I_2 signal during ~15 hours of exposure to both light and O_3
413 shows that 54% (82 nmol) of the original 152 nmol of I^- remained unreacted in the frozen solution despite the signal
414 apparently stabilizing at its baseline. A similar calculation cannot be performed for the pH ≤ 2 experiments because
415 of the inability to accurately quantify the amount of I_2 lost during connection of the flowtube to the CIMS. It is
416 therefore probable that a significant number of the ions, as well as H_2O_2, exist within brine channels within the ice
417 (Bartels-Rausch et al., 2014; Malley et al., 2018), such that oxidation chemistry is occurring throughout the ice. The
418 diffusion rates of the product molecular halogens through bulk ice are likely slow, such that only surface production
419 is observed here (Abbatt et al., 2012). Henry's Law constants suggest that I_2 not at the ice surface will transfer to the
420 air more slowly than other molecular halogens due to having a higher solubility (41.9 M/atm and 8.4 M/atm at -20 ºC
421 for I_2 and Br_2. respectively) (Raso et al., 2017). Consequently, upon irradiation, OH radicals will react with the most
422 oxidizable ion via R8-12 (e.g., I^-). Of the halogens produced from frozen solutions here, it is expected that I_2 is
423 observed most readily given the high polarizability and surface affinity of I^- in aqueous solutions (Gladich et al., 2011),
424 and the relative ease of oxidation of I^-. That is, surface concentrations will be relatively enhanced with larger, more
425 polarizable anions ($I^- > Br^- > Cl^-$) (Gladich et al., 2011), which favors production of I_2 over Br_2, and Br_2 over Cl_2. As
426 the larger/more reactive ions are depleted through oxidation, the next largest ion then becomes more favorably
427 oxidized. This implies that, if the larger anion is enhanced at the surface, the calculated relative rate constants do not
428 accurately represent fundamental relative reactivity, but rather the effective relative reactivity given knowledge of the
429 bulk composition. However, the observed relative oxidation rate constants are consistent with the standard reduction
430 potentials (tendency to become oxidized) for I^-, Br^-, and Cl^-, i.e. 0.620, 1.098, and 1.360V for I_2, Br_2, and Cl_2,
431 respectively (Chemical Rubber Company and Lide, 2005).

432 Despite these relative oxidation rates, molecular halogen levels have been previously observed at
433 concentrations within the snowpack interstitial air within two orders of magnitude of each other. At Utqiaġvik, AK,
434 snowpack Br_2 has been observed under artificial radiation at peak levels of 1100 pmol mol^{-1} (Custard et al., 2017), I_2
435 up to 50 pmol mol^{-1} (Raso et al., 2017) , and Cl_2 up to 20 pmol mol^{-1} (Custard et al., 2017) under artificial irradiation.
436 Though there are substantially lower natural abundances of I^- (Raso et al., 2017), I_2 is still observed at levels
437 comparable to / approaching those typical of Cl_2 and Br_2. The relative rate constants (ease of X^- oxidation by OH
438 radicals) we calculate would then appear to explain that the reactivity of the larger ions (which incorporates

439 components of surface affinity and chemical reactivity to OH) compensate for the low abundances, possibly leading
440 to comparable production rates in our laboratory experiments, and comparable snowpack gas phase concentrations.

441 Using a modified version of Eq. (1), we can estimate relative in situ OH-mediated halogen production rates
442 using published halide ratios from melted in situ snow samples from Utqiaġvik, AK (Eq. (2)).

443 $$\frac{\frac{d[X_2]}{dt}}{\frac{d[Y_2]}{dt}} = \frac{k_{X^-}[X^-][OH][H^+]}{k_{Y^-}[Y^-][OH][H^+]} \quad (2)$$

444 For a range of possible values, we utilize previously published, minimum and maximum $[Br^-]/[Cl^-]$ values that include
445 corresponding X_2 observations (i.e., halide ratios from samples that were shown to photochemically produce X_2):
446 0.0005 ± 0.0001 (Custard et al., 2017) and 0.026 ± 0.008 (Pratt et al., 2013). These ratios yield a corresponding range
447 for $\frac{\frac{d[Br_2]}{dt}}{\frac{d[Cl_2]}{dt}}$ of 180 ± 20 to 6000 ± 2000. $\frac{\frac{d[I_2]}{dt}}{\frac{d[Br_2]}{dt}}$ can additionally be estimated from Raso et al. (2017), where $[I^-]/[Br^-]$
448 ranges from 0.00040 ± 0.00003 to 0.129 ± 0.006, calculated $\frac{\frac{d[I_2]}{dt}}{\frac{d[Br_2]}{dt}}$ values range from 3.3 ± 1.5 to 1200 ± 500. While
449 simultaneous production of I_2 and Cl_2 was not observed herein, k_{I^-}/k_{Cl^-} can be calculated by multiplying k_{I^-}/k_{Br^-} by k_{Br^-}
450 $/k_{Cl^-}$. Therefore, for $[I^-]/[Cl^-]$ ranging from (1.0 ± 0.1) x 10^{-6} to (1.5 ± 0.1) x 10^{-4} (Raso et al., 2017), we obtain $\frac{\frac{d[I_2]}{dt}}{\frac{d[Cl_2]}{dt}}$
451 values of (2 ± 1) x 10^3 to (3 ± 2) x 10^5. The results of these calculations indicate that the observed relative rates of
452 production more than compensate for the relative halide ion abundances.

453 However, the observed relative rates of production are inconsistent with the observed relative snowpack
454 interstitial air X_2 abundances from field observations, which show similar (within a factor of 10) abundances in
455 irradiated snowpack interstitial air. We can formulate the following hypotheses to explain this:

456 1. There exist important competing loss processes for Br_2 and I_2 after initial production.

457 2. Other Cl_2 production pathways account for the majority of ambient concentrations.

458 Concerning hypothesis 1, one likely loss process includes aqueous inter-halogen partitioning, as in R25 (where X = I
459 or Br, and Y = I, Br, or Cl):

460 $$X_2 + Y^- \leftrightarrow X_2Y^- \leftrightarrow XY + X^- \quad (R28)$$

461 Evidence supporting this possibility include the photochemical formation of IBr in concert with photochemical Br_2
462 production during low pH experiments (in Fig. 2b), as has been observed previously (Abbatt et al., 2010; Sjostedt and
463 Abbatt, 2008). In addition, photolysis of X_2 is faster for the larger molecular halogens. Thompson et al., (2015) report

464 J_{X_2} = 0.15, 0.044, and 0.0021 s^{-1} for I_2, Br_2, and Cl_2, respectively during solar noon in March at Utqiaġvik, AK,
465 corresponding to photolytic lifetimes of 7s, 23s, and 476s, respectively. Thus, faster photolysis of the larger halogens
466 in the snowpack air will contribute to levelling the production rate differences, given penetration of actinic radiation
467 into the snowpack (King and Simpson, 2001). Evidence also exists in support hypothesis 2, possibly via the
468 heterogeneous recycling involved in the halogen explosion mechanism outlined in Sect. 1. Wang and Pratt (2017)
469 discuss that Br_2 and Cl_2 in ambient air at Utqiaġvik have opposite diurnal trends, indicating different governing
470 mechanisms for each molecular halogen species. We discuss this in greater detail in Sect. 4.2.

471 **4.2 The role of O_3 in enhancing halogen production**

472 In experiments without an OH source, I_2 production amounts were greatest after O_3 was introduced to the
473 illuminated tube for both pH regimes (Table 2). This likely results from a combination of heterogeneous recycling,
474 and the surface and aqueous reactions between O_3 and I^- ($k = 2.0 \times 10^{-12}$ cm^3 $molecules^{-1}$ s^{-1} (Liu et al., 2001)). While
475 O_3-mediated halogen production has been observed directly from frozen surfaces in previous laboratory studies
476 (Artiglia et al., 2017; Oldridge and Abbatt, 2011; Oum et al., 1998a; Wren et al., 2013), Br_2 was not observed to be
477 produced from the Arctic snowpack without irradiation (Pratt et al., 2013). This discrepancy raises a question of the
478 role of O_3 in initial halogen release in the Arctic spring.

479 In the presence of light, O_3 was found to stimulate additional I_2 and Br_2 production in the experiments herein,
480 as discussed in Sect 3.4. This additional production could result from a combination of the following mechanisms.
481 First, as discussed above, O_3 can react with halides on frozen saline surfaces to produce Br_2 or I_2 per reactions R18-
482 19, and then R4 (Artiglia et al., 2017; Carpenter et al., 2013; Gladich et al., 2015; Hayase et al., 2010; Oum et al.,
483 1998a; Shaw and Carpenter, 2013; Wren et al., 2013). It is possible that Br_2 (as well as other halogens) may have
484 been produced via this mechanism at levels below the LOD in previous Arctic snowpack studies (Custard et al., 2017;
485 Pratt et al., 2013; Raso et al., 2017); however, this may provide sufficient levels of Br_2 to enrich the snowpack in Br^-
486 to drive the photochemical production mechanism upon radiation. Second, given a flow tube residence time of 12
487 seconds, gas phase production of HOX is possible and could potentially enhance X_2 production, given a timescale for
488 molecular diffusion of 6.5 seconds for HOBr from the center of the tube to the ice surface. At this flow rate, there is
489 enough time for 1-2 heterogeneous reaction cycles. Consistent with this recycling mechanism, we observed HOI, and
490 HOBr at low pH (Fig. 3-4).

Revisiting the pathways for Cl_2 production from Sect. 4.1, there is growing evidence for the role of heterogeneous chemistry. Recently, Wren et al. (2013) observed substantial Cl_2 production from their artificial snow samples in the presence of both O_3 and light, invoking the "halogen explosion" mechanism (Sect. 1). In this scenario, HOI or HOBr could liberate Cl from the "disordered interface" to produce ICl or BrCl, which can undergo R1-4 to produce HOCl that ultimately oxidizes Cl^- to produce Cl_2. Liao et al. (2014) observed results consistent with this mechanism above the snowpack in Utqiaġvik, AK, reporting a strong correlation between Cl_2, O_3, and solar radiation; similarly, Custard et al. (2016) observed ClO correlated with Cl_2. This pathway is certainly viable for producing Cl_2 in our experiments, given there is enough time for recycling.

5 Summary and Conclusions

We show here that the hydroxyl radical can act as an effective condensed-phase halide oxidant leading to I_2, IBr, Br_2, and Cl_2 production under acidic conditions. Rates of release were dictated by both pH and relative halide concentrations. The molecular halogen produced appears to be highly influenced by which ions are enhanced at the ice surface, with I_2 production occurring prior to Br_2 production, which commenced after the $[I^-]/[Br^-]$ was reduced. An opportunity exists to further explore this chemistry via surface-sensitive methods, for which recent developments have been shown to effectively enable characterization of the surface composition of frozen solutions of sodium chloride under near atmospherically relevant conditions (Artiglia et al., 2017; Orlando et al., 2016). It would be useful to confirm the dominant ions involved in this surface-based chemistry over time. Further investigations into the effects of halide ratios on halogen production are also suggested, including measurements of how the ratios vary for different frozen Arctic surfaces, as well as how they vary spatially. While condensed-phase OH produces Br_2 and I_2 most rapidly in this study, it appears that other mechanisms, such as heterogeneous recycling of HOCl or $ClONO_2$, could be a more dominant mechanism for in situ production of gas phase Cl_2 (Wang and Pratt, 2017). We find the addition of O_3 provides additional production of at least Br_2 and I_2, probably through gas-phase production of HOX or $XONO_2$ and subsequent halogen explosion chemistry. These results lend support for the photochemical mechanisms proposed by the recent in situ snowpack experiments (Custard et al., 2017; Pratt et al., 2013; Raso et al., 2017) in which condensed-phase OH chemistry provides seed halogens that subsequently undergo heterogeneous recycling in order to build up atmospheric concentrations of halogens.

The pH dependence of halogen activation necessitates study on the pH on relevant Arctic frozen surfaces. Pratt et al. (2013) found that the frozen surfaces most conducive to in situ photochemical Br_2 production had acidic pH after melting, while no production was observed from those with a well-buffered alkaline ice brine. Similarly, we find herein that condensed-phase OH-induced halogen production is enhanced at lower pH. Wren and Donaldson (2012a, 2012b) found in laboratory studies that pH of acidic and basic solutions remains essentially unchanged after freezing, and that saline solutions with buffers (i.e., seawater) maintain their buffering capacity following trace gas deposition, supporting the lack of observed Br_2 production from the sea ice surface (Pratt et al., 2013). Therefore, it would be useful to test in situ production of halogens from Arctic frozen surfaces in tandem with the testing of the pH of said surfaces in order to determine the atmospherically relevant surface pH range required for halogen production.

Data availability. The data analysed in this work have been submitted for deposit onto the National Science Foundation Arctic Data Center (arcticdata.io) for public accessibility. Until they are published, data are available upon e-mail request to the first author (halfacre@ius.edu).

Author contributions. JWH and PBS designed the research and JWH performed the experiments and data analysis. All authors contributed to the discussion and interpretation of the results and writing of the paper.

Competing interests. The authors declare that they have no conflict of interest.

Acknowledgements

We would like to thank the National Science Foundation for their funding (PLR-1417668 and PLR-1417906, OPP-1417668). We also express thanks to J. H. Slade, L. G. Huey, D. J. Tanner, F. Xiong, A. R. W. Raso, and K. D. Custard for their assistance with CIMS operation and maintenance. Additionally, we thank the Purdue Chemistry Shop for helping build both the cooling and photolysis boxes, as well as the Jonathan Amy Facility for Chemical Instrumentation for their support in the fabrication of the experimental flow tube and setup of our experimental boxes. Thanks are also extended to M. Haas and M. Bischoff for performing total organic carbon analysis of our samples,

542 and A. R. W. Raso for confirmation of the iodide concentrations in our Instant Ocean samples. Finally, we thank T.
543 Miller and the Purdue Birck Nanotechnology Center for the provision of the nano-grade water used for our samples.

544 **References**

545 Abbatt, J., Oldridge, N., Symington, A., Chukalovskiy, V., McWhinney, R. D., Sjostedt, S. and Cox, R. A.: Release
546 of Gas-Phase Halogens by Photolytic Generation of OH in Frozen Halide−Nitrate Solutions: An Active Halogen
547 Formation Mechanism?, J. Phys. Chem. A, 114(23), 6527–6533, doi:10.1021/jp102072t, 2010.
548 Abbatt, J. P. D., Thomas, J. L., Abrahamsson, K., Boxe, C., Granfors, A., Jones, A. E., King, M. D., Saiz-Lopez, A.,
549 Shepson, P. B., Sodeau, J., Toohey, D. W., Toubin, C., von Glasow, R., Wren, S. N. and Yang, X.: Halogen activation
550 via interactions with environmental ice and snow in the polar lower troposphere and other regions, Atmos Chem Phys,
551 12(14), 6237–6271, doi:10.5194/acp-12-6237-2012, 2012.
552 Artiglia, L., Edebeli, J., Orlando, F., Chen, S., Lee, M.-T., Corral Arroyo, P., Gilgen, A., Bartels-Rausch, T., Kleibert,
553 A., Vazdar, M., Andres Carignano, M., Francisco, J. S., Shepson, P. B., Gladich, I. and Ammann, M.: A surface-
554 stabilized ozonide triggers bromide oxidation at the aqueous solution-vapour interface, Nat. Commun., 8(1),
555 doi:10.1038/s41467-017-00823-x, 2017.
556 Barrie, L. and Platt, U.: Arctic tropospheric chemistry: an overview, Tellus B, 49(5), 450–454, doi:10.1034/j.1600-
557 0889.49.issue5.2.x, 1997.
558 Bartels-Rausch, T., Jacobi, H.-W., Kahan, T. F., Thomas, J. L., Thomson, E. S., Abbatt, J. P. D., Ammann, M.,
559 Blackford, J. R., Bluhm, H., Boxe, C., Domine, F., Frey, M. M., Gladich, I., Guzmán, M. I., Heger, D., Huthwelker,
560 T., Klán, P., Kuhs, W. F., Kuo, M. H., Maus, S., Moussa, S. G., McNeill, V. F., Newberg, J. T., Pettersson, J. B. C.,
561 Roeselová, M. and Sodeau, J. R.: A review of air–ice chemical and physical interactions (AICI): liquids, quasi-liquids,
562 and solids in snow, Atmos Chem Phys, 14(3), 1587–1633, doi:10.5194/acp-14-1587-2014, 2014.
563 Carpenter, L. J., MacDonald, S. M., Shaw, M. D., Kumar, R., Saunders, R. W., Parthipan, R., Wilson, J. and Plane, J.
564 M. C.: Atmospheric iodine levels influenced by sea surface emissions of inorganic iodine, Nat. Geosci., 6(2), 108–
565 111, doi:10.1038/ngeo1687, 2013.
566 Chemical Rubber Company and Lide, D. R., Eds.: CRC handbook of chemistry and physics: a ready-reference book
567 of chemical and physical data, 86. ed., CRC Press, Boca Raton., 2005.

568 Cho, H., Shepson, P. B., Barrie, L. A., Cowin, J. P. and Zaveri, R.: NMR Investigation of the Quasi-Brine Layer in
569 Ice/Brine Mixtures, J. Phys. Chem. B, 106(43), 11226–11232, doi:10.1021/jp020449+, 2002.
570 Custard, K. D., Pratt, K. A., Wang, S. and Shepson, P. B.: Constraints on Arctic Atmospheric Chlorine Production
571 through Measurements and Simulations of Cl_2 and ClO, Environ. Sci. Technol., 50(22), 12394–12400,
572 doi:10.1021/acs.est.6b03909, 2016.
573 Custard, K. D., Raso, A. R. W., Shepson, P. B., Staebler, R. M. and Pratt, K. A.: Production and Release of Molecular
574 Bromine and Chlorine from the Arctic Coastal Snowpack, ACS Earth Space Chem., 1(3), 142–151,
575 doi:10.1021/acsearthspacechem.7b00014, 2017.
576 Fickert, S., Adams, J. W. and Crowley, J. N.: Activation of Br_2 and BrCl via uptake of HOBr onto aqueous salt
577 solutions, J. Geophys. Res. Atmospheres, 104(D19), 23719–23727, doi:10.1029/1999JD900359, 1999.
578 France, J. L., Reay, H. J., King, M. D., Voisin, D., Jacobi, H. W., Domine, F., Beine, H., Anastasio, C., MacArthur,
579 A. and Lee-Taylor, J.: Hydroxyl radical and NO_x production rates, black carbon concentrations and light-absorbing
580 impurities in snow from field measurements of light penetration and nadir reflectivity of onshore and offshore coastal
581 Alaskan snow, J. Geophys. Res., 117, doi:10.1029/2011JD016639, 2012.
582 Garland, J. A. and Curtis, H.: Emission of iodine from the sea surface in the presence of ozone, J. Geophys. Res.,
583 86(C4), 3183, doi:10.1029/JC086iC04p03183, 1981.
584 Gladich, I., Shepson, P. B., Carignano, M. A. and Szleifer, I.: Halide Affinity for the Water−Air Interface in Aqueous
585 Solutions of Mixtures of Sodium Salts, J. Phys. Chem. A, 115(23), 5895–5899, doi:10.1021/jp110208a, 2011.
586 Gladich, I., Francisco, J. S., Buszek, R. J., Vazdar, M., Carignano, M. A. and Shepson, P. B.: Ab Initio Study of the
587 Reaction of Ozone with Bromide Ion, J. Phys. Chem. A, 119(19), 4482–4488, doi:10.1021/jp5101279, 2015.
588 Hayase, S., Yabushita, A., Kawasaki, M., Enami, S., Hoffmann, M. R. and Colussi, A. J.: Heterogeneous Reaction of
589 Gaseous Ozone with Aqueous Iodide in the Presence of Aqueous Organic Species, J. Phys. Chem. A, 114(19), 6016–
590 6021, doi:10.1021/jp101985f, 2010.
591 Hellebust, S., Roddis, T. and Sodeau, J. R.: Potential Role of the Nitroacidium Ion on HONO Emissions from the
592 Snowpack, J. Phys. Chem. A, 111(7), 1167–1171, doi:10.1021/jp068264g, 2007.
593 Herring, J. R. and Liss, P. S.: A new method for the determination of iodine species in seawater, Deep Sea Res.
594 Oceanogr. Abstr., 21(9), 777–783, doi:10.1016/0011-7471(74)90085-0, 1974.

595 Kim, K., Yabushita, A., Okumura, M., Saiz-Lopez, A., Cuevas, C. A., Blaszczak-Boxe, C. S., Min, D. W., Yoon, H.-
596 I. and Choi, W.: Production of Molecular Iodine and Tri-iodide in the Frozen Solution of Iodide: Implication for Polar
597 Atmosphere, Environ. Sci. Technol., 50(3), 1280–1287, doi:10.1021/acs.est.5b05148, 2016.
598 Knipping, E. M., Lakin, M. J., Foster, K. L., Jungwirth, P., Tobias, D. J., Gerber, R. B., Dabdub, D. and Finlayson-
599 Pitts, B. J.: Experiments and Simulations of Ion-Enhanced Interfacial Chemistry on Aqueous NaCl Aerosols, Science,
600 288(5464), 301–306, doi:10.1126/science.288.5464.301, 2000.
601 Küpper, F. C., Schweigert, N., Gall, E. A., Legendre, J.-M., Vilter, H. and Kloareg, B.: Iodine uptake in Laminariales
602 involves extracellular, haloperoxidase-mediated oxidation of iodide, Planta, 207(2), 163–171,
603 doi:10.1007/s004250050469, 1998.
604 Liao, J., Huey, L. G., Tanner, D. J., Flocke, F. M., Orlando, J. J., Neuman, J. A., Nowak, J. B., Weinheimer, A. J.,
605 Hall, S. R., Smith, J. N., Fried, A., Staebler, R. M., Wang, Y., Koo, J.-H., Cantrell, C. A., Weibring, P., Walega, J.,
606 Knapp, D. J., Shepson, P. B. and Stephens, C. R.: Observations of inorganic bromine (HOBr, BrO, and Br_2) speciation
607 at Barrow, Alaska, in spring 2009, J. Geophys. Res. Atmospheres, 117(D14), D00R16, doi:10.1029/2011JD016641,
608 2012.
609 Liao, J., Huey, L. G., Liu, Z., Tanner, D. J., Cantrell, C. A., Orlando, J. J., Flocke, F. M., Shepson, P. B., Weinheimer,
610 A. J., Hall, S. R., Ullmann, K., Beine, H. J., Wang, Y., Ingall, E. D., Stephens, C. R., Hornbrook, R. S., Apel, E. C.,
611 Riemer, D., Fried, A., Mauldin Iii, R. L., Smith, J. N., Staebler, R. M., Neuman, J. A. and Nowak, J. B.: High levels
612 of molecular chlorine in the Arctic atmosphere, Nat. Geosci., 7(2), 91–94, doi:10.1038/ngeo2046, 2014.
613 Liu, Q., Schurter, L. M., Muller, C. E., Aloisio, S., Francisco, J. S. and Margerum, D. W.: Kinetics and Mechanisms
614 of Aqueous Ozone Reactions with Bromide, Sulfite, Hydrogen Sulfite, Iodide, and Nitrite Ions, Inorg. Chem., 40(17),
615 4436–4442, doi:10.1021/ic000919j, 2001.
616 Lockwood, A. L., Shepson, P. B., Fiddler, M. N. and Alaghmand, M.: Isoprene nitrates: preparation, separation,
617 identification, yields, and atmospheric chemistry, Atmos Chem Phys, 10(13), 6169–6178, doi:10.5194/acp-10-6169-
618 2010, 2010.
619 Luther, G. W., Swartz, C. B. and Ullman, W. J.: Direct determination of iodide in seawater by cathodic stripping
620 square wave voltammetry, Anal. Chem., 60(17), 1721–1724, doi:10.1021/ac00168a017, 1988.
621 Malley, P. P. A., Chakraborty, S. and Kahan, T. F.: Physical Characterization of Frozen Saltwater Solutions Using
622 Raman Microscopy, ACS Earth Space Chem., doi:10.1021/acsearthspacechem.8b00045, 2018.

McConnell, J. C., Henderson, G. S., Barrie, L., Bottenheim, J., Niki, H., Langford, C. H. and Templeton, E. M. J.: Photochemical bromine production implicated in Arctic boundary-layer ozone depletion, Nature, 355(6356), 150–152, doi:10.1038/355150a0, 1992.

Neuman, J. A., Nowak, J. B., Huey, L. G., Burkholder, J. B., Dibb, J. E., Holloway, J. S., Liao, J., Peischl, J., Roberts, J. M., Ryerson, T. B., Scheuer, E., Stark, H., Stickel, R. E., Tanner, D. J. and Weinheimer, A.: Bromine measurements in ozone depleted air over the Arctic Ocean, Atmos Chem Phys, 10(14), 6503–6514, doi:10.5194/acp-10-6503-2010, 2010.

O'Driscoll, P., Lang, K., Minogue, N. and Sodeau, J.: Freezing Halide Ion Solutions and the Release of Interhalogens to the Atmosphere, J. Phys. Chem. A, 110(14), 4615–4618, doi:10.1021/jp060491v, 2006.

O'Driscoll, P., Minogue, N., Takenaka, N. and Sodeau, J.: Release of Nitric Oxide and Iodine to the Atmosphere from the Freezing of Sea-Salt Aerosol Components, J. Phys. Chem. A, 112(8), 1677–1682, doi:10.1021/jp710464c, 2008.

Oldridge, N. W. and Abbatt, J. P. D.: Formation of Gas-Phase Bromine from Interaction of Ozone with Frozen and Liquid NaCl/NaBr Solutions: Quantitative Separation of Surficial Chemistry from Bulk-Phase Reaction, J. Phys. Chem. A, 115(12), 2590–2598, doi:10.1021/jp200074u, 2011.

Orlando, F., Waldner, A., Bartels-Rausch, T., Birrer, M., Kato, S., Lee, M.-T., Proff, C., Huthwelker, T., Kleibert, A., Bokhoven, J. van and Ammann, M.: The Environmental Photochemistry of Oxide Surfaces and the Nature of Frozen Salt Solutions: A New in Situ XPS Approach, Top. Catal., 1–14, doi:10.1007/s11244-015-0515-5, 2016.

O'Sullivan, D. and Sodeau, J. R.: Freeze-Induced Reactions: Formation of Iodine−Bromine Interhalogen Species from Aqueous Halide Ion Solutions, J. Phys. Chem. A, 114(46), 12208–12215, doi:10.1021/jp104910p, 2010.

Oum, K. W., Lakin, M. J. and Finlayson-Pitts, B. J.: Bromine activation in the troposphere by the dark reaction of O_3 with seawater ice, Geophys. Res. Lett., 25(21), 3923–3926, doi:10.1029/1998GL900078, 1998a.

Oum, K. W., Lakin, M. J., DeHaan, D. O., Brauers, T. and Finlayson-Pitts, B. J.: Formation of Molecular Chlorine from the Photolysis of Ozone and Aqueous Sea-Salt Particles, Science, 279(5347), 74–76, doi:10.1126/science.279.5347.74, 1998b.

Platt, U. and Hönninger, G.: The role of halogen species in the troposphere, Chemosphere, 52(2), 325–338, doi:10.1016/S0045-6535(03)00216-9, 2003.

649 Pratt, K. A., Custard, K. D., Shepson, P. B., Douglas, T. A., Pöhler, D., General, S., Zielcke, J., Simpson, W. R., Platt,
650 U., Tanner, D. J., Gregory Huey, L., Carlsen, M. and Stirm, B. H.: Photochemical production of molecular bromine
651 in Arctic surface snowpacks, Nat. Geosci., 6(5), 351–356, doi:10.1038/ngeo1779, 2013.
652 Raso, A. R. W., Custard, K. D., May, N. W., Tanner, D., Newburn, M. K., Walker, L., Moore, R. J., Huey, L. G.,
653 Alexander, L., Shepson, P. B. and Pratt, K. A.: Active molecular iodine photochemistry in the Arctic, Proc. Natl.
654 Acad. Sci., 114(38), 10053–10058, doi:10.1073/pnas.1702803114, 2017.
655 Saiz-Lopez, A. and von Glasow, R.: Reactive halogen chemistry in the troposphere, Chem. Soc. Rev., 41(19), 6448–
656 6472, doi:10.1039/C2CS35208G, 2012.
657 Shaw, M. D. and Carpenter, L. J.: Modification of Ozone Deposition and I_2 Emissions at the Air–Aqueous Interface
658 by Dissolved Organic Carbon of Marine Origin, Environ. Sci. Technol., 47(19), 10947–10954,
659 doi:10.1021/es4011459, 2013.
660 Simpson, W. R., von Glasow, R., Riedel, K., Anderson, P., Ariya, P., Bottenheim, J., Burrows, J., Carpenter, L. J.,
661 Frieß, U., Goodsite, M. E., Heard, D., Hutterli, M., Jacobi, H.-W., Kaleschke, L., Neff, B., Plane, J., Platt, U., Richter,
662 A., Roscoe, H., Sander, R., Shepson, P., Sodeau, J., Steffen, A., Wagner, T. and Wolff, E.: Halogens and their role in
663 polar boundary-layer ozone depletion, Atmos Chem Phys, 7(16), 4375–4418, doi:10.5194/acp-7-4375-2007, 2007.
664 Simpson, W. R., Brown, S. S., Saiz-Lopez, A., Thornton, J. A. and Glasow, R. von: Tropospheric Halogen Chemistry:
665 Sources, Cycling, and Impacts, Chem. Rev., 115(10), 4035–4062, doi:10.1021/cr5006638, 2015.
666 Sjostedt, S. J. and Abbatt, J. P. D.: Release of gas-phase halogens from sodium halide substrates: heterogeneous
667 oxidation of frozen solutions and desiccated salts by hydroxyl radicals, Environ. Res. Lett., 3(4), 045007,
668 doi:10.1088/1748-9326/3/4/045007, 2008.
669 Steffen, A., Douglas, T., Amyot, M., Ariya, P., Aspmo, K., Berg, T., Bottenheim, J., Brooks, S., Cobbett, F., Dastoor,
670 A., Dommergue, A., Ebinghaus, R., Ferrari, C., Gardfeldt, K., Goodsite, M. E., Lean, D., Poulain, A. J., Scherz, C.,
671 Skov, H., Sommar, J. and Temme, C.: A synthesis of atmospheric mercury depletion event chemistry in the
672 atmosphere and snow, Atmospheric Chem. Phys., 8(6), 1445–1482, doi:10.5194/acp-8-1445-2008, 2008.
673 Steffen, A., Bottenheim, J., Cole, A., Ebinghaus, R., Lawson, G. and Leaitch, W. R.: Atmospheric mercury speciation
674 and mercury in snow over time at Alert, Canada, Atmos Chem Phys, 14(5), 2219–2231, doi:10.5194/acp-14-2219-
675 2014, 2014.

676 Tang, T. and McConnell, J. C.: Autocatalytic release of bromine from Arctic snow pack during polar sunrise, Geophys.
677 Res. Lett., 23(19), 2633–2636, doi:10.1029/96GL02572, 1996.
678 Thompson, C. R., Shepson, P. B., Liao, J., Huey, L. G., Apel, E. C., Cantrell, C. A., Flocke, F., Orlando, J., Fried, A.,
679 Hall, S. R., Hornbrook, R. S., Knapp, D. J., Mauldin III, R. L., Montzka, D. D., Sive, B. C., Ullmann, K., Weibring,
680 P. and Weinheimer, A.: Interactions of bromine, chlorine, and iodine photochemistry during ozone depletions in
681 Barrow, Alaska, Atmospheric Chem. Phys., 15(16), 9651–9679, doi:10.5194/acp-15-9651-2015, 2015.
682 Tsunogai, S. and Sase, T.: Formation of iodide-iodine in the ocean, Deep Sea Res. Oceanogr. Abstr., 16(5), 489–496,
683 doi:10.1016/0011-7471(69)90037-0, 1969.
684 Vogt, R., Crutzen, P. J. and Sander, R.: A mechanism for halogen release from sea-salt aerosol in the remote marine
685 boundary layer, Nature, 383(6598), 327–330, doi:10.1038/383327a0, 1996.
686 Wang, S. and Pratt, K. A.: Molecular Halogens above the Arctic Snowpack: Emissions, Diurnal Variations, and
687 Recycling Mechanisms, J. Geophys. Res. Atmospheres, 2017.
688 Weaver, J. R.: Birck Nanotechnology Center Technical Overview, edited by Purdue University Office of Research
689 and Partnerships, [online] Available from: http://docs.lib.purdue.edu/gendes/5 (Accessed 28 January 2016), 2015.
690 Wennberg, P.: Atmospheric chemistry: Bromine explosion, Nature, 397(6717), 299–301, doi:10.1038/16805, 1999.
691 Wren, S. N. and Donaldson, D. J.: How does deposition of gas phase species affect pH at frozen salty interfaces?,
692 Atmospheric Chem. Phys., 12(21), 10065–10073, doi:https://doi.org/10.5194/acp-12-10065-2012, 2012a.
693 Wren, S. N. and Donaldson, D. J.: Laboratory Study of pH at the Air–Ice Interface, J. Phys. Chem. C, 116(18), 10171–
694 10180, doi:10.1021/jp3021936, 2012b.
695 Wren, S. N., Donaldson, D. J. and Abbatt, J. P. D.: Photochemical chlorine and bromine activation from artificial
696 saline snow, Atmos Chem Phys, 13(19), 9789–9800, doi:10.5194/acp-13-9789-2013, 2013.
697 Xiong, F., McAvey, K. M., Pratt, K. A., Groff, C. J., Hostetler, M. A., Lipton, M. A., Starn, T. K., Seeley, J. V.,
698 Bertman, S. B., Teng, A. P., Crounse, J. D., Nguyen, T. B., Wennberg, P. O., Misztal, P. K., Goldstein, A. H.,
699 Guenther, A. B., Koss, A. R., Olson, K. F., de Gouw, J. A., Baumann, K., Edgerton, E. S., Feiner, P. A., Zhang, L.,
700 Miller, D. O., Brune, W. H. and Shepson, P. B.: Observation of isoprene hydroxynitrates in the southeastern United
701 States and implications for the fate of NOx, Atmos Chem Phys, 15(19), 11257–11272, doi:10.5194/acp-15-11257-
702 2015, 2015.
703

Atmos. Chem. Phys. Discuss., https://doi.org/10.5194/acp-2018-757
Manuscript under review for journal Atmos. Chem. Phys.
Discussion started: 22 August 2018

Atmospheric Chemistry and Physics Discussions

705 **Tables**

706 Table 1: List of relevant species monitored by chemical ionization mass spectrometry ($I(H_2O)_n^-$ as reagent ion) with corresponding
707 *m/z* values.

Species	*m/z*
$I^{81}Br^-$	208
$I^{79}Br^{79}Br^-$	285
$I^{79}Br^{81}Br^-$	287
$I^{35}Cl^-$	162
$I^{37}Cl^-$	164
$I^{35}Cl^{35}Cl^-$	197
$I^{35}Cl^{37}Cl^-$	199
$I^{37}Cl^{37}Cl^-$	201
$I^{79}Br^{35}Cl^-$	241
$I^{81}Br^{35}Cl^-$ / $I^{79}Br^{37}Cl^-$	243
I_3^-	381
$IHO^{79}Br$	223
$IHO^{81}Br$	225
$IHO_3{}^5Cl^-$	179
$IHO_3{}^7Cl^-$	181
$IHOI^-$	271
$I^{79}IBr^-$	333
$I^{81}IBr^-$	335

708

709

Atmos. Chem. Phys. Discuss., https://doi.org/10.5194/acp-2018-757
Manuscript under review for journal Atmos. Chem. Phys.
Discussion started: 22 August 2018

Atmospheric Chemistry and Physics Discussions

Table 2: Results for all experiments performed. The first line in an experiment represents the integrated totals of molecular halogen production after 1 hour of irradiation (t = 0 through t =1 h). The results on italicized lines are 1 h integrated production amounts beginning once additional ozone was introduced to the flow tube. Average LODs across experiments were 1.8 ± 0.4, 1.2 ± 0.3, and 9 ± 2 pmol mol^{-1} for Br_2, Cl_2, and I_2 respectively. "IO#" represents samples composed of Instant Ocean, and "SW#" represents "saltwater" samples, composed of reagent salts. "CL1" here represents the experiment performed using 0.557M high purity NaCl.

Experiment	Oxidant	pH	I_2 produced (nmol)	Br_2 produced (nmol)	Cl_2 produced (nmol)
IO1	H_2O_2	4.7	9 (±3)	< LOD	
	+O_3		*22 (±8)*	*0.06 (±0.05)*	
IO2	H_2O_2	4.7	0.6 (±0.4)	0.034 (±0.003)	
	+O_3		*21 (±14)*	*0.038 (±0.003)*	
SW1	H_2O_2	4.7	6.0 (±2.1)	< LOD	
	+O_3		*51 (±19)*	*0.024(±0.014)*	
SW2	H_2O_2	4.5	8 (±4)	< LOD	
	+O_3		*51 (±25)*	*0.018 (±0.003)*	
IO3	NO_2^-	2.0	39 (±1)	0.084 (±0.002)	
IO4	H_2O_2	1.7	0.8 (±0.3)	5.6 (±0.3)	
	+O_3		*< LOD*	*12 (±1)*	
IO5	H_2O_2	1.7	0.33 (±0.11)	3.5 (±0.4)	
	+O_3		*0.11 (±0.04)*	*9.2 (±1.0)*	
SW3	NO_2^-	1.8	4.0 (±0.1)	< LOD	
	+O_3		*< LOD*	*0.46 (±0.1)*	
SW4	NO_2^-	2.2	< LOD	5.4 (±0.7)	
	+O_3		*< LOD*	*13 (±2)*	
SW5	H_2O_2	1.8	0.75 (±0.26)	6.0 (±0.7)	
	+O_3		*< LOD*	*15 (±2)*	
CL1	H_2O_2	1.8	0.10 (±0.03)	0.10 (±0.01)	0.093 (±0.008)
IO6	None	4.7	< LOD	< LOD	
	+O_3		*26 (±9)*	*0.015 (±0.001)*	
IO7	None	4.7	0.10 (±0.06)	< LOD	
	+O_3		*47 (±29)*	*0.012 (±0.001)*	
SW6	None	4.7	< LOD	< LOD	
	+O_3		*80 (±1)*	*0.16 (±0.01)*	
SW7	None	4.5	< LOD	< LOD	
	+O_3		*48 (±2)*	*0.023 (±0.001)*	
IO8	None	2.0	14 (±10)	< LOD	
	+O_3		*2.6 (±1.7)*	*0.14 (±0.02)*	
SW8	None	2.0	14 (±10)	< LOD	
	+O_3		*2.6 (±1.7)*	*0.14 (±0.02)*	

Atmos. Chem. Phys. Discuss., https://doi.org/10.5194/acp-2018-757
Manuscript under review for journal Atmos. Chem. Phys.
Discussion started: 22 August 2018

Atmospheric Chemistry and Physics Discussions

716 **Figures**

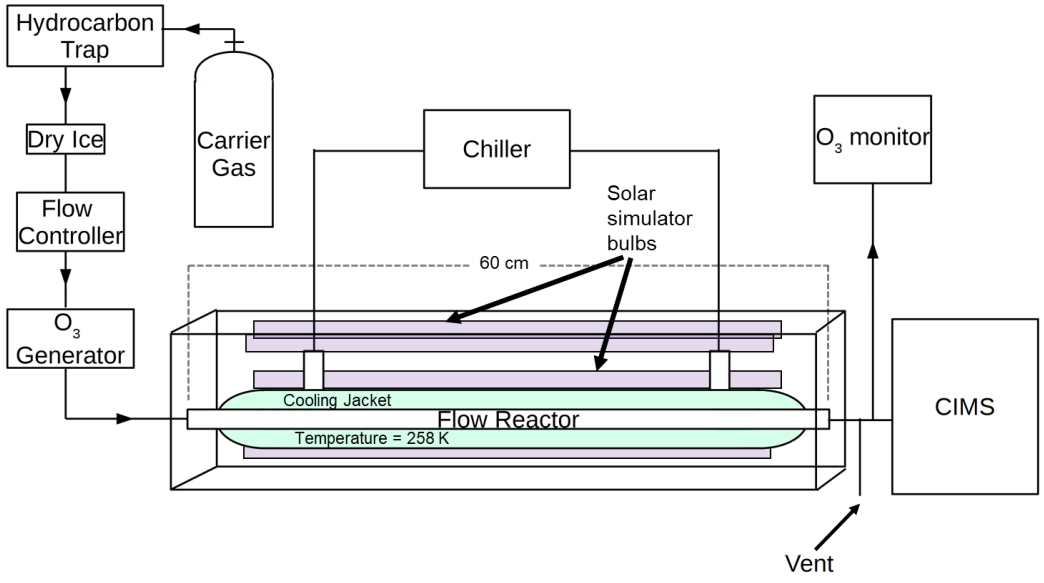

717

718 Figure 1: Experimental schematic. Purple bars represent powered solar simulator bulbs. The green shading around the flow tube
719 (flow reactor) represents cooling liquid (60% ethylene glycol, 40% water) circulated through the chiller. The flow reactor region
720 itself has an inner diameter of 2.5 cm.

721

Atmos. Chem. Phys. Discuss., https://doi.org/10.5194/acp-2018-757
Manuscript under review for journal Atmos. Chem. Phys.
Discussion started: 22 August 2018

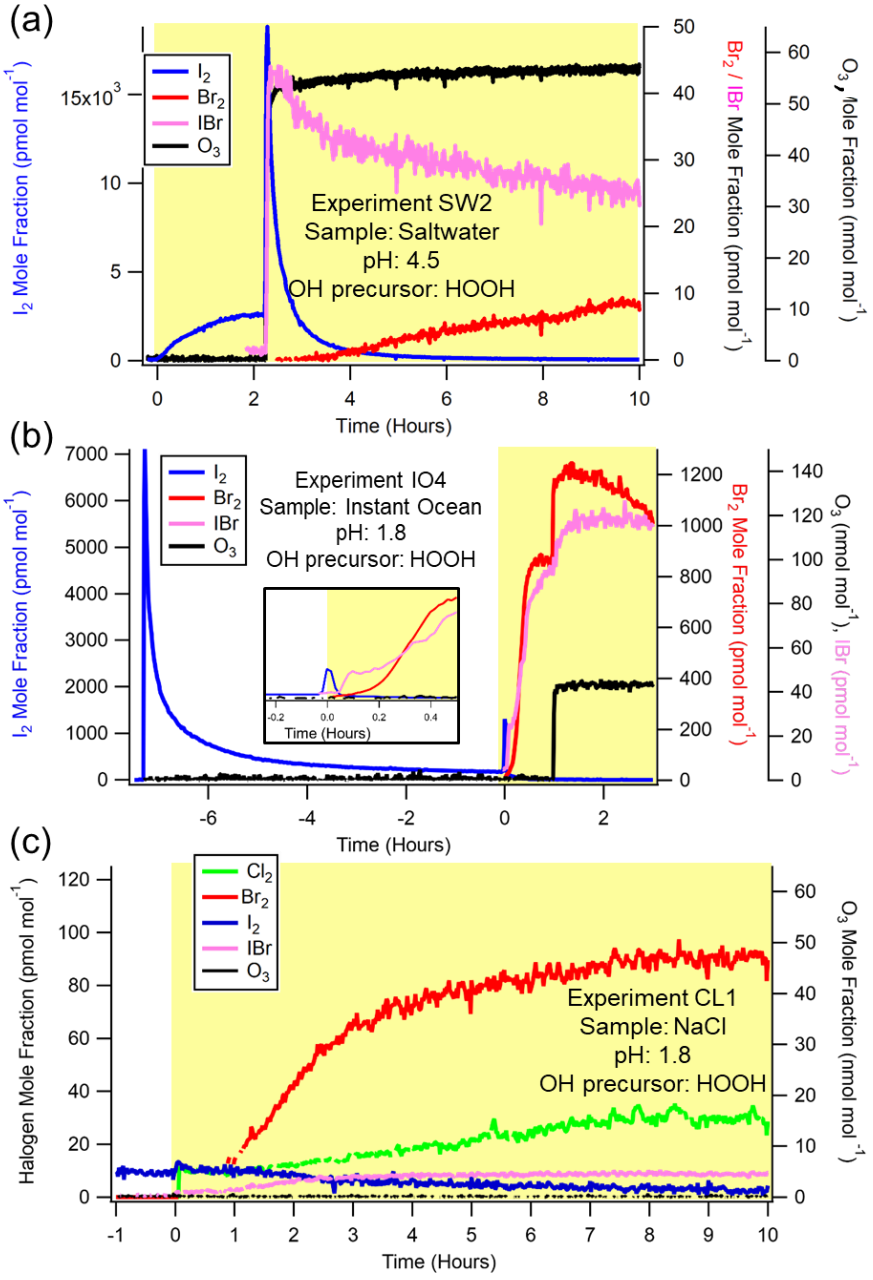

Figure 2: Representative experiments of OH-mediated production of X_2, and subsequent production of X_2 from O_3 addition. a) Saltwater experiment (SW2) at pH=4.5. b) Instant Ocean experiment (IO4) at pH = 1.8. Time varying Br_2 and IBr signals before t=0 are shown in Fig. S1. Inset more clearly shows the increase of I_2 signal after irradiation. c) NaCl experiment (CL1) at pH = 1.8. Timescale represents hours from the activation of the lights, and the yellow shading represents presence of radiation from solar simulator bulbs. Gaps in data represent periods when the isotopic ratios showed an interference.

Atmos. Chem. Phys. Discuss., https://doi.org/10.5194/acp-2018-757
Manuscript under review for journal Atmos. Chem. Phys.
Discussion started: 22 August 2018

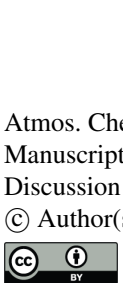

Atmospheric Chemistry and Physics Discussions

728

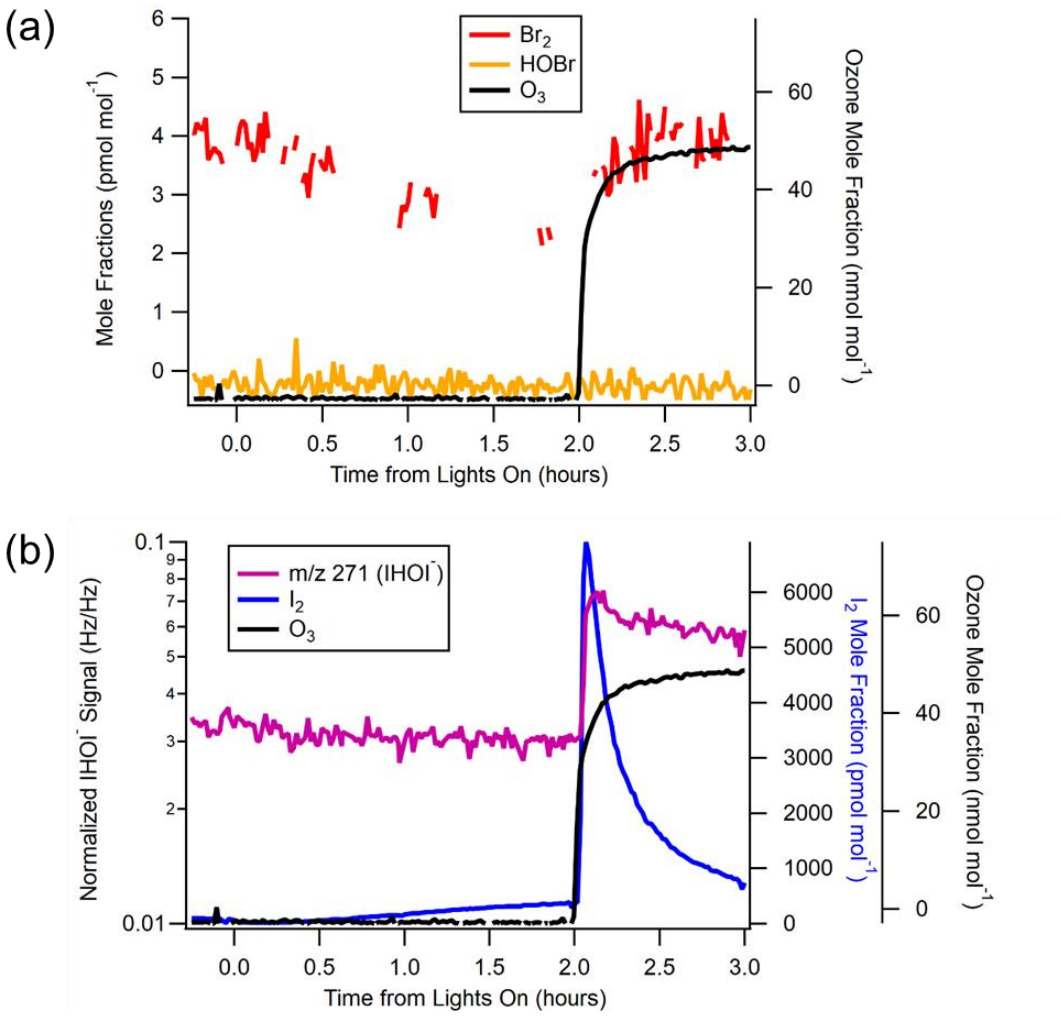

729

730 Figure 3: HOX signals from experiment IO2, pH=4.7. a) Comparison of Br_2 mole fractions to HOBr. Note that the HOBr signal,
731 while calibrated, should be used only for qualitative purposes as its identity could not be confirmed using isotopic ratios with *m/z*
732 223 due to its relatively large background signal. b) Effect of O_3 on I_2 and HOI.

733

Atmos. Chem. Phys. Discuss., https://doi.org/10.5194/acp-2018-757
Manuscript under review for journal Atmos. Chem. Phys.
Discussion started: 22 August 2018

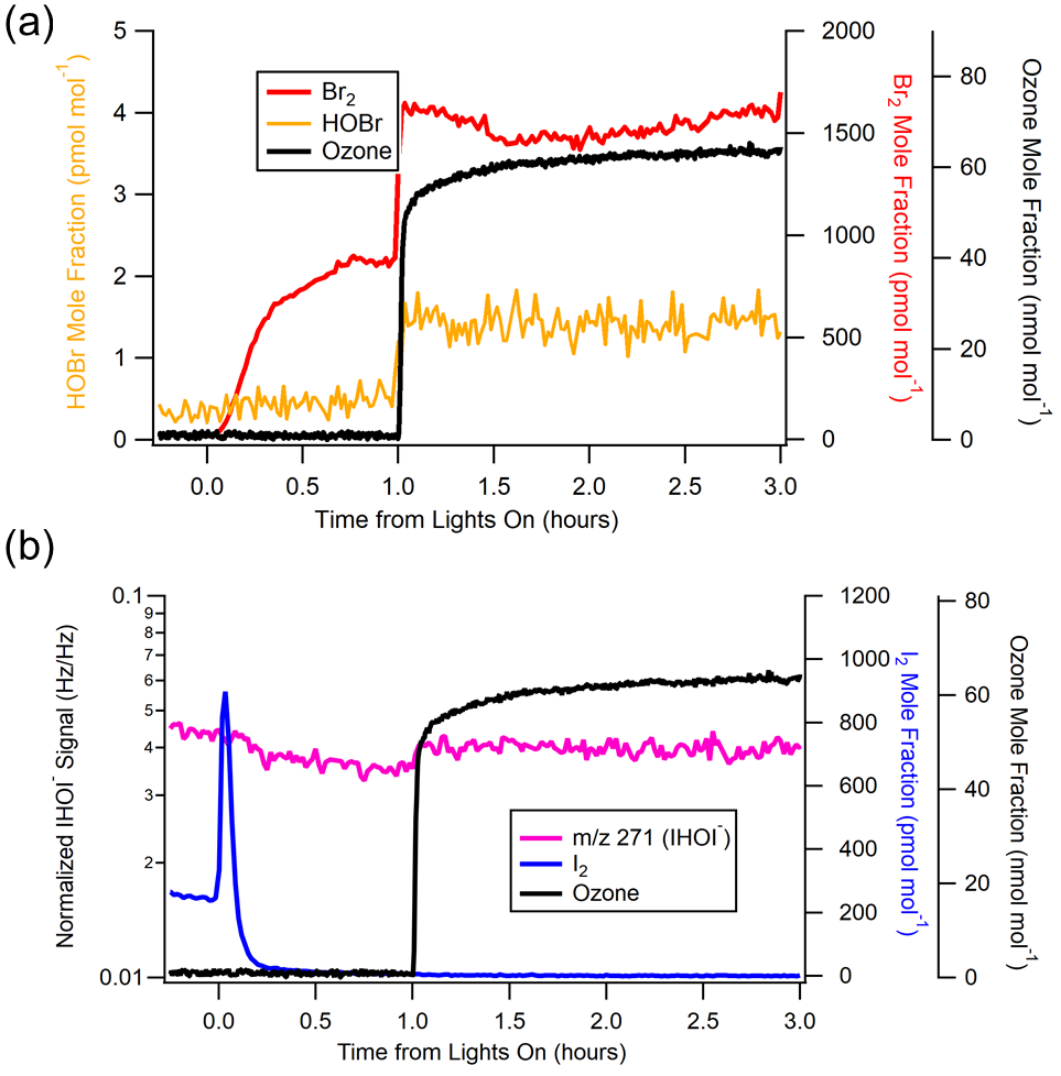

Figure 4: HOX signals from experiment SW5, pH=1.8. a) Comparison of Br_2 mole fractions to HOBr (*m/z* 225). Note that the HOBr signal, while calibrated, should be used only for qualitatively purposes as its identity could not be confirmed using isotopic ratios with *m/z* 223. b) Effect of O_3 on I_2 and HOI.